

Widely Tunable Separate Absorption and Modulation Wavelength Converter With Integrated Microwave Termination

Matthew M. Dummer, *Student Member, IEEE*, Matthew N. Sysak, *Member, IEEE, Member, OSA*, Anna Tauke-Pedretti, *Student Member, IEEE*, James W. Raring, *Member, IEEE, Member, OSA*, Jonathan Klamkin, *Student Member, IEEE*, and Larry A. Coldren, *Fellow, IEEE, Fellow, OSA*

Abstract—A widely tunable wavelength converter utilizing a separate absorption and modulation configuration and only dc bias connections is demonstrated. The device integrates an SG-DBR laser with a traveling-wave electroabsorption modulator and an optically pre-amplified receiver and introduces a simplified bias scheme by the inclusion of passive resistor and capacitor circuit elements. We discuss a the design of these passive elements and their compatibility with fabrication of photonic integrated circuits. The device demonstrates over 12 GHz optical bandwidth and error free 10 Gb/s wavelength conversion is achieved with less than 2.5 dB power penalty over 25 nm of output tuning.

Index Terms—Electroabsorption, optical receivers, optical transmitters, p-i-n photodiodes, sampled grating distributed Bragg reflector (SG-DBR), semiconductor optical amplifiers (SOAs), traveling wave devices, wavelength conversion (WC), wavelength division multiplexing (WDM).

I. INTRODUCTION

AS CURRENT optical fiber communications continue to push the limits of bandwidth utilization, wavelength conversion is becoming an increasingly important function in wavelength division multiplexed (WDM) networks. Wavelength conversion in high traffic networks reduces blocking probabilities, when signal contention is problematic, and has applications in optical routing, switching and add/drop multiplexing [1]. Monolithically integrated wavelength converters (WC), in which a tunable laser source can be incorporated on-chip, are particularly interesting devices due to their small footprint, low-cost packaging, and potential for scalability.

Although many technologies for wavelength conversion have been employed, there are two main approaches which lend themselves to monolithically integrated devices. The first of these is a carrier-modulated all-optical approach, in which an input signal is combined with a tunable laser source in the same semiconductor optical amplifier (SOA). If operated in the saturation regime, the inherent non-linearity of the

SOA provides cross gain (XGM) and cross phase modulation (XPM) to transfer the information from the input wavelength to the wavelength from the tunable source. The bandwidth of SOA-based WCs is limited by the carrier recovery lifetime of the SOAs, and operation has typically been limited to data rates up to 10 Gb/s [2], although faster operation has also been demonstrated with very high power penalties [3]. Recently, delayed interferometric techniques have been employed to surpass the carrier recovery lifetime limit and 40 Gb/s operation has been achieved in a monolithic device [4], [5].

The other approach to monolithic wavelength conversion, pursued in this work, is based on separate absorption and modulation (SAM) of the optical signals. In this approach, a tunable transmitter and optical receiver are monolithically integrated on a single-chip. The photodiode of the receiver is interconnected to the modulator of the transmitter, which can be either a Mach-Zehnder (MZ) or electroabsorption modulator (EAM). The input signal into the receiver is optically pre-amplified using an SOA such that sufficient photocurrent is generated in the photodiode to directly drive the modulator without any electronic driver circuitry. With this configuration, the input data can be transcribed onto any output wavelength within the range of the tunable source. SAM-WCs have demonstrated wavelength conversion up to 10 Gb/s [6] and have potential for higher bit rate scaling, as similar configurations used in optical gates have already demonstrated functionality up to 500 Gb/s [7]. Other advantages of SAM-WCs include lower power dissipation and smaller footprint than their SOA-based counterparts, reshaping and re-amplification (2R) of the input data signal [8], and the elimination of any output optical filtering requirement, since the two optical signals are spatially separated throughout the entire device. The potential for 3R regeneration has also been demonstrated by including clock recovery circuitry for retiming [8]. However, previous demonstrations of SAM-WCs have been complicated by the transport of microwave signals off of the chip requiring high speed probes, bias-Ts [6], and complex bias circuitry [9]. In this paper, we demonstrate an EAM based SAM-WC in which a termination resistor and dc-blocking capacitor are integrated onto the chip, such that only a common dc bias is required for the both EAM and photodiode and no additional RF components are necessary. By keeping all high frequency components confined to the chip, this advancement greatly simplifies the packaging requirements and allows for operation and scalability of SAM-WCs which is

Manuscript received April 18, 2007; revised November 16, 2007. This work was supported by the Defense Advanced Research Projects Agency (DARPA) under MTO-LASOR Grant W911NF-04-9-0001 and MTO-CS-WDM Grant N66001-02-C-8026.

The authors are with the Department of Electrical and Computer Engineering and the Department of Materials, University of California Santa Barbara, Santa Barbara, CA 93106 USA (e-mail: dummer@engineering.ucsb.edu).

Color versions of one or more of the figures in this paper are available online at <http://ieeexplore.ieee.org>.

Digital Object Identifier 10.1109/JLT.2007.915202

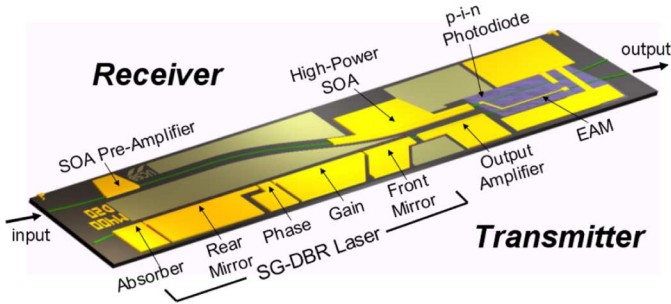


Fig. 1. Schematic of the monolithically integrated wavelength converter with separate receiver and tunable transmitter. The total device footprint is 3.1 mm by 0.5 mm.

analogous to SOA-based implementations while maintaining all the benefits of a separate absorption and modulation device.

II. WAVELENGTH CONVERTER DESIGN

This device is fabricated using the dual quantum well (DQW) integration platform described in [10], which incorporates a 350 nm quaternary (InGaAsP) waveguide layer between p- and n-type InP cladding layers above and below, respectively. The DQW consists of a set of seven offset quantum wells (QWs) with a photoluminescence peak wavelength (λ_{PL}) of 1542 nm above the waveguide layer and eight detuned quantum wells ($\lambda_{PL} = 1455$ nm) centered in the waveguide. The offset wells provide the optical gain for the laser and SOA components and are selectively etched from passive and modulation regions before blanket regrowth of the p-type InP cladding. The centered wells are present throughout the device and are used for EAM efficiency under reverse bias but are detuned from the operating wavelength to maintain low optical loss throughout the unbiased passive regions.

Fig. 1 depicts the full the SAM-WC consisting of two spatially separated surface-ridge waveguides which function as the receiver and transmitter. The receiver consists of two SOAs followed by a quantum well p-i-n photodiode (PIN-PD). The first SOA is 200 μm long and 3 μm wide and the second SOA is 800 μm long and with a ridge that flares linearly to 9 μm over the last half of the length. The flared ridge design has been shown to improve the saturation power of the SOA by reducing optical power density within the waveguide [11]. An S-bend between the two receiver SOAs was designed to minimize the interconnect distance between the PIN-PD and the EAM. The PIN-PD is 20 μm long and utilizes the offset QW stack as the absorbing layer for generating photocurrent. The ridge width is tapered from 9–6.5 μm to prevent saturation from excess space charge while minimizing the total capacitance.

The transmitter consists of a widely tunable sampled grating distributed Bragg reflector (SG-DBR) laser followed by an output 400 μm long SOA and 400 μm long EAM. The SG-DBR and SOA ridge width is 3.5 μm and tapers to a 2.5 μm in the EAM. Photo-BCB (Benzo-cyclobutene) is defined around the EAM and PIN-PD as a low-k dielectric to reduce parasitic capacitance. A 75 μm long electrical interconnect above the BCB connects the PIN-PD to the EAM (Fig. 2). The interconnect and PIN-PD and EAM electrodes are designed as microstrip transmission lines and configured such that the

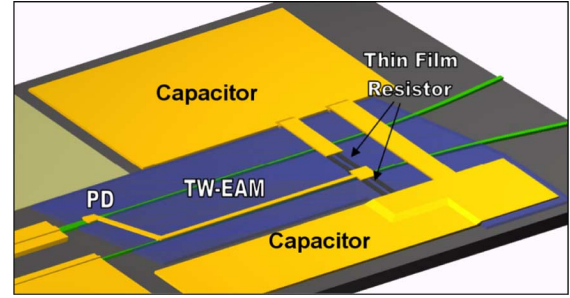


Fig. 2. Schematic of integrated photodiode and EAM with on chip load resistor and dc-blocking capacitor.

optical and electrical signals propagate in the same direction to take advantage of traveling wave effects. The EAM electrode is terminated by an on-chip resistor and dc blocking capacitor described in detail in Section III.

III. PASSIVE COMPONENTS

The resistor and capacitor elements function to terminate the generated microwave signals after being transported from the absorption to modulation regions. The load resistance directly determines the magnitude of the electric field in the EAM, and hence the conversion efficiency, as well as the total operating bandwidth of the device. Power handling is also important, as the resistor must be capable sinking all the photocurrent generated in both the PIN-PD and EAM. For this work, NiCr thin film resistors were chosen because of their ease of fabrication and patterning with standard liftoff techniques. It is well known that electron beam evaporation of NiCr alloyed sources produces varying sheet resistance, and poor repeatability due to the differing vapor pressures of nickel and chrome during deposition [12]. To ensure controllable composition and repeatability we have instead developed a digital layer deposition technique where nickel and chrome sources are evaporated separately and then alloyed by annealing. For the initial run of devices, four layers totaling 720 \AA were deposited with a composition of 70:30 Nickel-Chrome followed by an anneal at 390 C. These resistors were patterned as either 1.25 or 2.5 squares with stripe lengths of 40 μm . This first run exhibited a low sheet resistance of 10 Ω/\square and poor power handling capability with breakdown occurring for dc biases greater than 1 V. On subsequent fabrication runs the resistor pattern dimensions were increased by 2.5 times to improve power handling and an eight layer deposition process was used to improve the uniformity of the alloy composition. For the same thickness, NiCr composition, and anneal temperature, the resistivity was increased to 14 Ω/\square as shown in Fig. 3. The eight-layer resistors also demonstrated better ohmic behavior and sustained biases greater than 2 V dc. These results have been repeated in three further fabrications.

As shown in Fig. 2 the resistor is followed by two metal-insulator-metal (MIM) capacitors on either sides of the ridges that provide a low impedance ground path for the microwave signal and allow for biasing of the EAM and PIN-PD. A 3500 \AA thick n-contacting AuGe ground plane extends from below the BCB to form the lower plate of the capacitor. The dielectric material consists of 2500 \AA of silicon nitride deposited by physical evaporation chemical vapor deposition (PECVD). A 2.5 μm thick

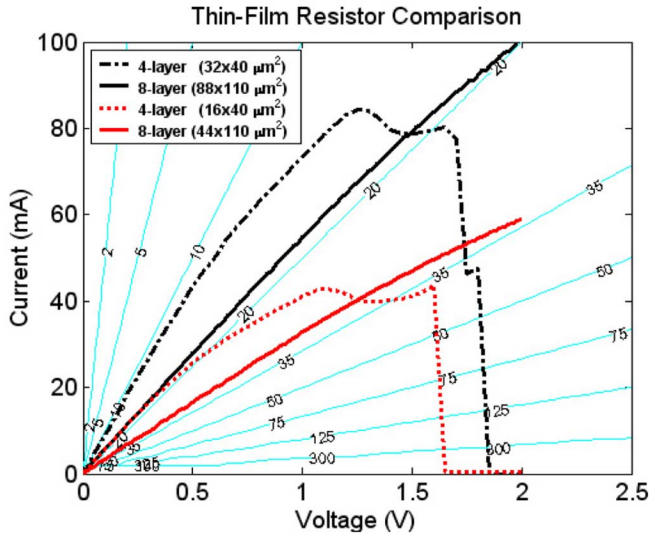


Fig. 3. Comparison of resistance and power handling for two NiCr resistor fabrications. Run 1 and 2 are denoted four layer and eight layer, respectively. Physical resistor dimensions are listed in parenthesis. Constant resistance contours are shown for reference.

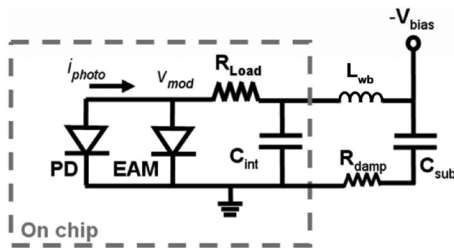


Fig. 4. Equivalent circuit diagram of wavelength converter.

gold layer forms the top plate of the capacitor and the interconnect to the NiCr resistor. The total area of the two on-chip capacitors is 0.14 mm^2 with a capacitance that has been measured to be 30 pF .

IV. BIASING

A circuit diagram depicting the bias configuration for the wavelength converter is shown in Fig. 4. Only a single reverse bias, applied through wirebonds to the two plates of the capacitor, is needed for biasing both the EAM and PIN-PD. Since both plates are equivalently “RF ground,” this bias scheme eliminates any parasitic capacitance typically associated with bonding pads and the need for any transmission lines or bias-Ts off chip. Also, placing the resistor in series with the two diodes ensures no dc power dissipation in the load resistor under normal reverse bias operation, aside from the dc photocurrent generated in the EAM. Though simplistic, this bias circuit also has two issues which need to be addressed. First, the 30 pF on chip capacitor (C_{int}) is a sufficient ground for frequencies above 600 MHz . However typically a larger capacitor ($C_{\text{sub}} = 220 \text{ nF}$) is added to the carrier to extend the low frequency response. This is especially important for achieving minimal pattern dependence for pseudo random bit streams with long word lengths. Second, the wirebonds from the carrier to the on-chip capacitor induce an LC resonance in the frequency response. Fig. 5 shows a simulation

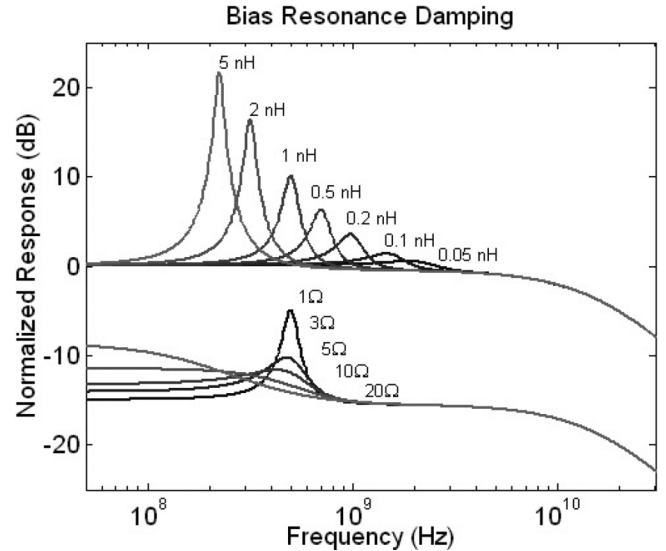


Fig. 5. Simulated effects of wirebond resonance on wavelength converter frequency response for various wirebond inductances (top) and damping resistor values (bottom).

of the small signal response for different values of wirebond inductance (L_{wb}). By minimizing the wirebond length and adding a small amount of series resistance to dampen the inductive peak (R_{damp}), the resonance can be effectively eliminated. Typically R_{damp} values used range from 3 to 5Ω for wirebonds less than 2 mm . Larger resistance values are avoided since they create a non-uniform response by effectively increasing the termination resistance for low frequency components.

V. RECEIVER PERFORMANCE

The receiver and transmitter have been extensively characterized separately to determine their individual contributions to wavelength converter performance. Due to the use of compressively strained QWs, the SOAs and PIN-PD are highly polarization sensitive and the input signal must be optimized to the transverse electric (TE) orientation to achieve the best performance. Both high gain and saturation power of the receiver SOAs are key attributes for achieving conversion gain and high extinction ratios. Fig. 6 shows the optical output power (P_{out}) versus input power (P_{in}) of the receiver for both SOAs biased at a current density of 6 kA/cm^2 . The continuous wave (CW) measurements show the receiver optical gain to be 19 dB when operating in the linear regime. The 1-dB output compression power of the receiver is 14 dBm , which translates into 25 mA of dc photocurrent generation. The modal absorption coefficient of the offset QWs under reverse bias has been measured by photocurrent spectroscopy to be 450 cm^{-1} , yielding an internal quantum efficiency of 60% for the $20 \mu\text{m}$ long PIN-PD. Small signal frequency response measurements demonstrate a 3-dB bandwidth in excess of 20 GHz for the PIN-PD with 25Ω termination. With sufficient bias, the tapered ridge PIN-PD design exhibits excellent power handling capabilities [11]. As shown in Fig. 7, with 14 mA average photocurrent the device shows no bandwidth degradation due to saturation effects for reverse biases greater than 2.5 V .

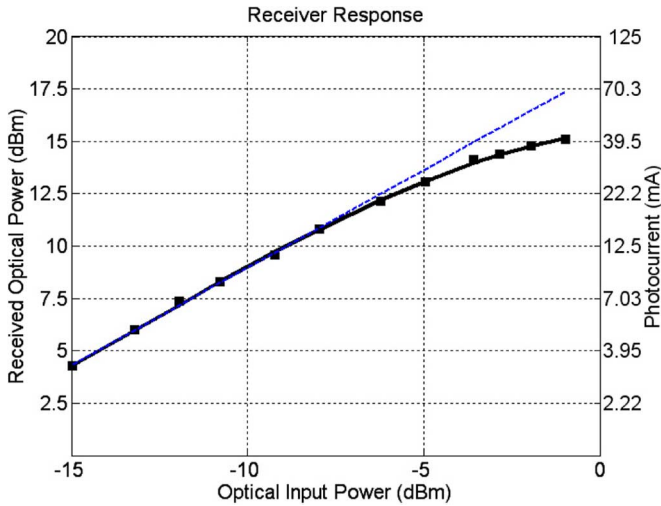


Fig. 6. Optical output power (P_{out}) vs optical input power (P_{in}) for biases of 40 mA and 290 mA on 200 μm and 800 μm SOAs, respectively. The measured photocurrent level from the PIN-PD is shown on the right axis. PIN-PD bias was -3.0 V.

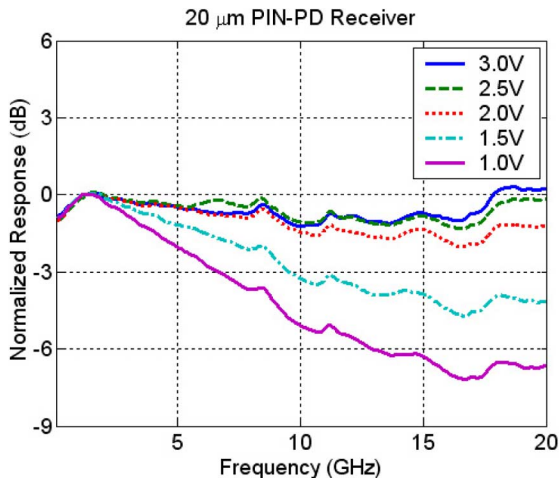


Fig. 7. Frequency response of 20 μm long PIN-PD photodetector for varying reverse bias with 25 Ω termination. The input power into the receiver was -6.7 dBm and average detected photocurrent was 14 mA.

VI. TRANSMITTER PERFORMANCE

The SG-DBR laser utilizes vernier tuning of the front and rear mirrors to achieve continuous tuning of the emission wavelength from 1522–1565 nm. The maximum fiber coupled output power is 6.2–9.8 dBm over the wavelength range of the SG-DBR for bias currents of 150 mA applied to both the gain section of the laser and the output SOA. dc extinction curves for the 400 μm long EAM are shown in Fig. 8 for wavelength between 1522 nm and 1559 nm. The detuned band edge of the centered quantum wells creates a strong wavelength dependence with peak slope efficiencies that range from 25 dB/V for the shortest wavelength down to 10 dB/V for longest wavelength.

Since the positions of the laser source and electrical termination in the wavelength converter are fixed, it is impossible to determine the amount of traveling wave (TW) benefit in the EAM directly. Instead, discrete TW-EAMs were fabricated on the same wafer as the integrated wavelength converter to

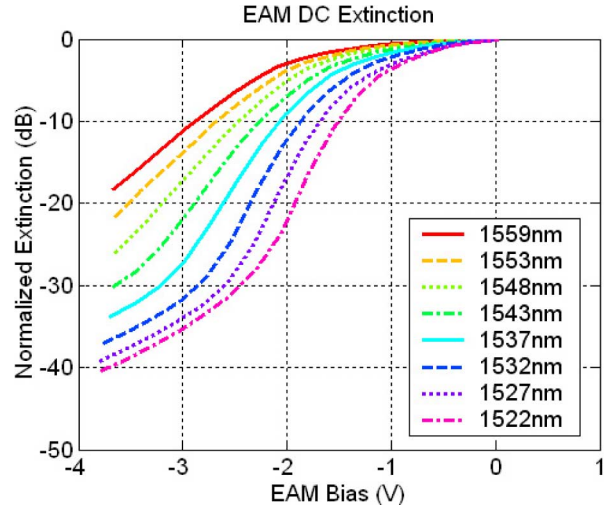


Fig. 8. DC extinction curves taken from 400 μm EAM over the tuning range of the SG-DBR.

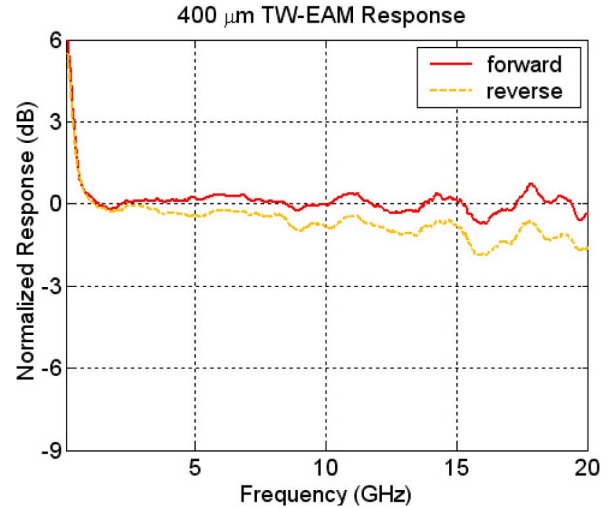


Fig. 9. Forward and reverse EO traveling wave response for the discrete 400 μm EAM. On-chip termination is 20 Ω . The dc bias is -2.0 V.

measure the electrical-to-optical (EO) response. These EAMs were directly driven by probing a coplanar waveguide (CPW) and terminated by the same on-chip resistor and capacitor. EO small signal measurements were performed using an external 1550 nm laser source coupled into either facet to compare co- and counter-propagating TW bandwidth. The characteristic impedance of the EAM transmission line was measured as 24 Ω and the NiCr resistor value used was 20 Ω to minimize electrical reflections in the device. These low impedances are typical of such capacitively loaded electrode structures [13], [14]. Fig. 9 shows results of the EO measurements comparing the “forward” response, when the optical signal propagates in the same direction as the electrical drive, and “reverse,” when the two signals counter-propagate. Although the 3-dB bandwidth is greater than 20 GHz in both cases, the forward measurement exhibits virtually no roll-off over the measurement range, which demonstrates the significance of the traveling wave design. The dc bias for both of these measurements was -2.0 V, although other experiments show that the response is independent of

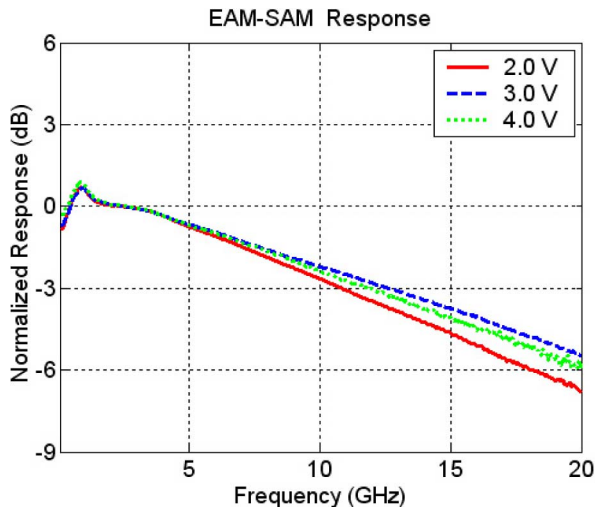


Fig. 10. Optical-to-optical small signal frequency response for SAM-WC for various reverse biases of EAM and PIN-PD. Load resistor is 35 Ω .

bias for typical operating points between -1.5 and 3.5 V. The sharp rise in the response below 1 GHz shows the limit of the integrated capacitor, since no external capacitor was used during this experiment.

VII. WAVELENGTH CONVERTER EXPERIMENTS

A series of experiments have been performed to evaluate wavelength conversion performance. For these experiments, the device under test was mounted and wirebonded to an aluminum nitride carrier. The carrier was placed on a copper stage with a temperature actively maintained at 16° C. A dc probe card contacting the carrier was used to apply all biases and optical signals were coupled to and from the chip using conically tipped lensed fibers. In all experiments, the input signal was amplified by an erbium doped fiber amplifier (EDFA) followed by an optical filter to reduce amplified spontaneous emission (ASE) noise and a polarization controller to optimize the receiver gain.

Testing of the wavelength converter consisted of both small and large signal characterization. First, small signal measurements were taken to determine the total optical-to-optical (OO) bandwidth of the device. The results of the small signal frequency response measurement are shown in Fig. 10 for varying bias. For -3 V bias and 35 Ω on-chip termination, the 3-dB optical bandwidth of the wavelength converter is 12.6 GHz.

Large signal experiments consisted of measuring the bit error rate (BER) of the device for wavelength conversion of digital data at 10 Gb/s with non-return-to-zero (NRZ) format. The BER test setup was similar to the one described in [15] and utilized a $2^{31} - 1$ pseudo-random bit stream (PRBS) as the input signal. Bit error rate curves were generated by attenuating the output of the device and measuring the BER for various powers into a commercial optical receiver.

A. Dynamic Range Experiments

The dynamic range of the SAM-WC receiver greatly affects the wavelength converter performance. Low input powers result in insufficient photocurrent levels for driving the EAM causing

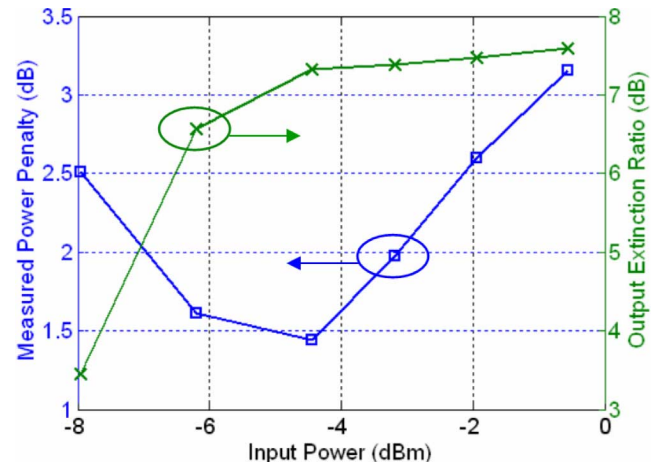


Fig. 11. Wavelength converted power penalty (at BER = 10^{-9}) and output extinction ratio for varied input powers. The input wavelength is 1548 nm and the output wavelength is 1537 nm. The EAM and PIN-PD bias is -2.5 V.

poor output extinction ratios (ER). Conversely, high input powers result in output pattern dependence due to saturation of the receiver SOA. Because of this, it was necessary to find the optimum input power for the device by measuring the BER at several input power levels. The bias currents for this experiment were fixed at 40 and 240 mA for the receiver SOAs, and 100 and 40 mA for the laser gain section and transmitter SOA, respectively. For fixed input and output wavelengths of 1548 and 1537 nm, the BER of the wavelength converted signal was compared with the BER for back-to-back transmission and the difference was calculated as a power penalty.

Fig. 11 shows the results of varying the optical input power into the wavelength converter. The measured power penalty at a BER of 10^{-9} along with the associated output extinction ratio is plotted for each input power. The power penalty reaches a minimum of 1.4 dB at the input power of -4.5 dBm. The explanation for this is best seen in the output eye diagrams in Fig. 12. Each eye, (a)–(f), is the wavelength converted output corresponding to the data points in Fig. 11 from left to right. For low input powers, (a) and (b), the BER is limited by the reduced output extinction ratio. For higher input powers, (d)–(f), the power penalty increases even though the output ER continues to improve. In this case, signal distortion due to the receiver SOA saturation becomes the limiting factor. The effect of the pattern dependence in the eye diagrams is apparent in the rising crossover point, and increased jitter and fall time that can be attributed to gain recovery time in the saturated receiver SOA.

The results of this experiment show that the optimum input power into the wavelength converter, -4.5 dBm, matches the 1-dB compression point of the receiver SOA from Fig. 6. The eye labeled (c) represents the optimum output with 7.3 dB extinction and 0.3 mW output amplitude. This value corresponds to unity conversion gain after accounting for 4 dB fiber coupling losses. Higher conversion efficiency is possible by increasing the bias current in the transmitter SOA to boost the output power. However, this comes at the expense of increased thermal crosstalk between the transmitter and receiver SOAs which reduces the maximum achievable receiver power.

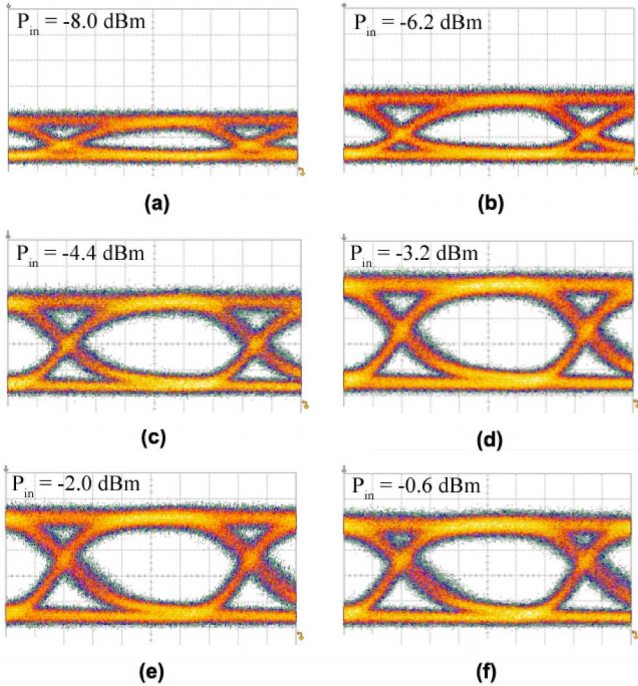


Fig. 12. 10 Gb/s wavelength converted (1548–1537 nm) eye diagrams corresponding to the input powers (P_{in}) in Fig. 11. The scales of the two axes are 16.3 ps/div and $95 \mu\text{W}/\text{div}$.

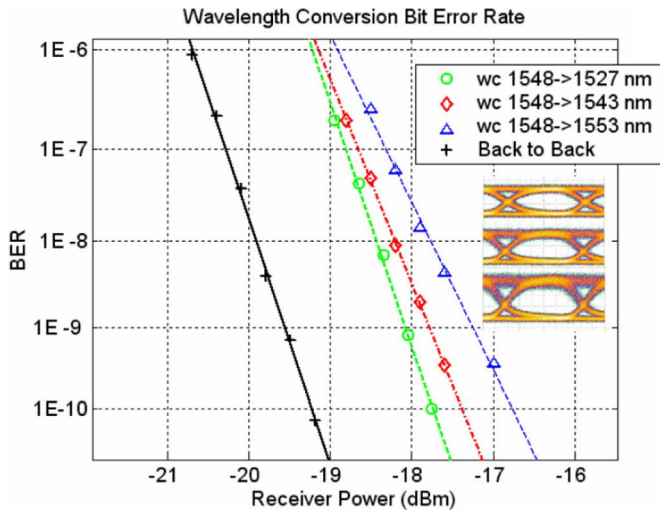


Fig. 13. Wavelength conversion BER measurements for constant input and varying output wavelength compared with back-to-back transmission. The corresponding eye diagrams are shown for 1527, 1543, and 1553 nm from top to bottom with extinction ratios of 8.0, 7.4, and 6.6 dB, respectively.

B. Wavelength Conversion Performance

After an optimal input power was determined, wavelength conversion was performed from the same fixed wavelength (1548 nm) to multiple output wavelengths across the tuning range of the SGDBR. The bias for the EAM and PIN-PD was adjusted to take advantage of the steepest slope efficiency of the modulator at each wavelength (Fig. 8). BER curves were generated at multiple wavelengths and again compared to back-to-back transmission to compute the conversion power penalty. The results of these wavelength conversion experiments are shown in Fig. 13. The dc bias was to -2.2 V , -2.9 V , and -3.2 V for the wavelengths of 1527, 1543, and 1553 nm,

respectively. The input power in to the device was -4.5 dBm and the output powers were -6.0 , -5.2 , and -4.0 dBm , respectively, after subtracting 4 dB fiber coupling losses from both facets. The extinction ratio of the wavelength converted signal ranges from 8.0–6.6 dB. Using a 2 s gating period, error-free operation was observed for all wavelengths with less than 2.5 dB power penalty compared with back-to-back transmission. The decrease in power penalty with shorter output wavelengths in this device is attributed to the increase in output extinction ratio [16]. Therefore, the digital performance could be improved by optimizing the design and band-edge detuning of the modulator quantum wells to achieve higher slope efficiency at the longer wavelengths.

VIII. CONCLUSION

SAM-WCs offer a low-power, small-footprint, bit rate scalable solution for wavelength conversion in WDM networks. We have presented the design, fabrication, and characterization of the first EAM-based widely tunable separate absorption and modulation wavelength converter with integrated passive circuit elements for terminations and biasing. This monolithically integrated device requires only dc connections to the InP chip, greatly reducing biasing and packaging complexity. Wavelength conversion at 10 Gbps demonstrated error free performance with power penalties of less than 2.5 dB over 25 nm of output wavelength tuning. The device performance can be further optimized by improving the linearity of the receiver SOAs, as well as increasing the efficiency of both the photodiode and EAM. These improvements in conjunction with an optimized traveling wave architecture should provide bit rate scaling to accommodate much higher data rates in the future.

REFERENCES

- [1] S. Yoo, "Wavelength conversion technologies for WDM network applications," *J. Lightwave Technol.*, vol. 14, no. 6, pp. 955–966, 1996.
- [2] M. Masanovic, V. Lal, J. Summers, J. Barton, E. Skogen, L. Rau, L. Coldren, and D. Blumenthal, "Widely tunable monolithically integrated all-optical wavelength converters in InP," *J. Lightwave Technol.*, vol. 23, no. 3, pp. 1350–1362, 2005.
- [3] T. Hatta, T. Miyahara, Y. Miyazaki, K. Takagi, K. Matsumoto, T. Aoyagi, K. Motoshima, K. Mishina, A. Maruta, and K. Kitayama, "Polarization-insensitive monolithic 40-Gbps SOA MZI wavelength converter with narrow active waveguides," *IEEE J. Sel. Topics Quantum Electron.*, vol. 13, pp. 32–39, 2007.
- [4] V. Lal, M. Masanovic, J. Summers, L. Coldren, and D. Blumenthal, "Performance optimization of an InP-based widely tunable all-optical wavelength converter operating at 40 Gb/s," *IEEE Photon. Technol. Lett.*, vol. 18, no. 4, pp. 577–579, 2006.
- [5] P. Bernasconi, W. Yang, L. Zhang, N. Sauer, L. Buhl, I. Kang, S. Chandrasekhar, and D. Neilson, "40 Gbit/s RZ wavelength converter in a monolithically integrated chip with a tunable laser," *Electron. Lett.*, vol. 41, no. 12, pp. 701–702, 2005.
- [6] M. Sysak, J. Raring, J. Barton, M. Dummer, A. Tauke-Pedretti, H. Poulsen, D. Blumenthal, and L. Coldren, "Single-chip, widely-tunable 10 Gbit/s photocurrent-driven wavelength converter incorporating a monolithically integrated laser transmitter and optical receiver," *Electron. Lett.*, vol. 42, no. 11, pp. 657–658, 2006.
- [7] S. Kodama, T. Yoshimatsu, and H. Ito, "500 Gbit/s optical gate monolithically integrating photodiode and electroabsorption modulator," *Electron. Lett.*, vol. 40, no. 9, pp. 555–556, 2004.
- [8] M. Sysak, J. Raring, L. Johansson, H. Poulsen, J. Barton, D. Blumenthal, and L. Coldren, "Optical 2R and 3R signal regeneration in combination with dynamic wavelength switching using a monolithically integrated, widely tunable photocurrent driven wavelength converter," in *Proc. Eur. Conf. Optical Communication (ECOC)*, Cannes, France, Sep. 2006, p. Th3.4.1.

- [9] J. S. Barton, M. N. Sysak, A. Tauke-Pedretti, M. Dummer, J. Raring, L. A. Johansson, M. L. Masanovic, D. J. Blumenthal, and L. A. Coldren, *Field Modulated Wavelength Converters*, L. A. Eldada and E. Lee, Eds. : SPIE, 2006, vol. 6124, pp. 612417–612417.
- [10] M. Sysak, J. Raring, J. Barton, M. Dummer, D. Blumenthal, and L. Coldren, "A single regrowth integration platform for photonic circuits incorporating tunable SGDBR lasers and quantum-well EAMS," *IEEE Photon. Technol. Lett.*, vol. 18, no. 15, pp. 1630–1632, 2006.
- [11] A. Tauke-Pedretti, M. Dummer, J. Barton, M. Sysak, J. Raring, and L. Coldren, "High saturation power and high gain integrated photoreceivers," *IEEE Photon. Technol. Lett.*, vol. 17, no. 10, pp. 2167–2169, 2005.
- [12] R. F. Kopf, R. Melendes, D. C. Jacobson, A. Tate, M. A. Melendes, R. R. Reyes, R. A. Hamm, Y. Yang, J. Frackoviak, N. G. Weimann, H. L. Maynard, and C. T. Liu, "Thin-film resistor fabrication for InP technology applications," *J. Vacuum Sci. Technol. B: Microelectron. Nanometer Structures*, vol. 20, no. 3, pp. 871–875, 2002.
- [13] G. Li, S. Pappert, P. Mages, C. Sun, W. Chang, and P. Yu, "High-saturation high-speed traveling-wave InGaAsP-InP electroabsorption modulator," *IEEE Photon. Technol. Lett.*, vol. 13, no. 10, pp. 1076–1078, 2001.
- [14] R. Lewen, S. Irmscher, and U. Eriksson, "Microwave cad circuit modeling of a traveling-wave electroabsorption modulator," *IEEE Trans. Microw. Theory Tech.*, vol. 51, no. 4, pp. 1117–1128, 2003.
- [15] M. Sysak, J. Barton, L. Johansson, J. Raring, E. Skogen, M. Masanovic, D. Blumenthal, and L. Coldren, "Single-chip wavelength conversion using a photocurrent-driven EAM integrated with a widely tunable sampled-grating DBR laser," *IEEE Photon. Technol. Lett.*, vol. 16, no. 9, pp. 2093–2095, 2004.



Matthew M. Dummer (S'06) received the B.S. degree in electrical engineering from the University of Minnesota, Twin Cities, in 2002, and M.S. degree from the University of California, Santa Barbara, in 2004, where he is current working toward the Ph.D. degree.

His research focuses on high functionality photonic integrated circuits for wavelength conversion. He also specializes in the fabrication of high power semiconductor optical amplifiers and photodiodes, as well as traveling wave circuit design for electroabsorption modulators.

electroabsorption modulators.



Matthew N. Sysak (M'06) received the B.S. degree in chemical engineering from the Pennsylvania State University, University Park, in 1998, and the M.S. and Ph.D. degrees from the University of California, Santa Barbara, in 2002 and 2005, respectively. His Ph.D. dissertation focused on material design as well as device design, fabrication, and testing of monolithically integrated, widely tunable, optoelectronic wavelength converters and signal regenerators.

He is currently working on novel photonic circuit design and fabrication for analog, phase modulated links. He has authored and coauthored over 30 conference and journal papers.

Dr. Sysak is a member of the Optical Society of America (OSA), Washington, DC, and the International Society for Optical Engineering (SPIE), Bellingham, WA.



Anna Tauke-Pedretti (S'02) received the B.S. degree in physics and electrical engineering from the University of Iowa, Iowa City, in 2001 and the M.S. degree from the University of California, Santa Barbara, in 2002, where she is currently working toward the Ph.D. degree.

Her current research interests focus on InP-based photonic integrated circuits for high-speed wavelength conversion. She has also developed monolithic high-speed transmitters and high-saturation power pre-amplified receivers.



James W. Raring (M'03) received the B.S. degree from California Polytechnic State University, San Luis Obispo, in 2001 and the Ph.D. degree in materials science from the University of California, Santa Barbara, in 2006. His dissertation focused on the design, growth, and fabrication of high-functionality wavelength agile photonic integrated circuits operating at 10 and 40 Gb/s. The photonic circuits were based on sampled grating DBR lasers, electroabsorption modulators, semiconductor optical amplifiers, and photodiodes.

His work explores novel integration methods coupling quantum-well intermixing with straightforward MOCVD regrowth steps. He has authored or coauthored over 70 technical papers.

Dr. Raring is a member of the Optical Society of America (OSA), Washington, DC, and the International Society for Optical Engineering (SPIE), Bellingham, WA.



Jonathan Klamkin (S'04) received the B.S. degree in electrical and computer engineering from Cornell University, Ithaca, NY, in 2002 and the M.S. degree in electrical and computer engineering from the University of California, Santa Barbara (UCSB), in 2004, where he is currently working toward the Ph.D. degree.

His research interests include the design, growth, fabrication, and characterization of widely-tunable semiconductor lasers, photodetectors, optical intensity and phase modulators, and semiconductor

optical amplifiers for InP based photonic integrated circuits. Currently his efforts are focused on novel coherent integrated receivers for highly linear fiber-optic links.



Larry A. Coldren (F'82) received the Ph.D. degree in electrical engineering from Stanford University, Stanford, CA, in 1972.

After 13 years in the research area at Bell Laboratories, he joined the University of California, Santa Barbara (UCSB), in 1984, where he is now the Fred Kavli Professor of Optoelectronics and Sensors, and the Director of the Optoelectronics Technology Center. In 1990, he cofounded Optical Concepts, later acquired as Gore Photonics, to develop novel vertical cavity surface-emitting laser (VCSEL) technology and in 1998 he cofounded Agility Communications to develop widely tunable integrated transmitters. At Bell Laboratories, he initially worked on waveguided surface-acoustic wave signal processing devices and coupled-resonator filters. He later developed tunable coupled-cavity lasers using novel reactive-ion etching (RIE) technology that he created for the then new InP-based materials. At UCSB he continued work on multiple-section tunable lasers, inventing, in 1988, the widely tunable multielement mirror concept. During the late 1980s, he also developed efficient vertical-cavity multiple-quantum-well modulators, which led to novel VCSEL designs that provided unparalleled levels of performance. His current research interests include developing new photonic integrated circuit (PIC) and VCSEL technology, including the underlying materials growth and fabrication techniques, creation of vertical and in-plane GaN-based emitters, efficient all-epitaxial InP-based VCSELs, and a variety of PICs incorporating numerous optical elements for widely tunable integrated transmitters, receivers, and wavelength converters. He has authored or coauthored over 700 papers, five book chapters, one textbook, and is a holder of 36 patents.

Prof. Coldren is a Fellow of the Optical Society of America (OSA), Washington, DC, and the Institution of Engineering and Technology (IET), London, U.K., and a member of the National Academy of Engineering. He was the recipient of the 2004 John Tyndall Award. He has presented dozens of invited and plenary talks at major conferences.